JTTEE5 20:344–350
DOI: 10.1007/s11666-010-9570-4
1059-9630/$19.00 © ASM International

Peer Reviewed

Microstructure and Electrochemical Behavior of Fe-Based Amorphous Metallic Coatings Fabricated by Atmospheric Plasma Spraying

Z. Zhou, L. Wang, D.Y. He, F.C. Wang, and Y.B. Liu

(Submitted April 30, 2010; in revised form August 17, 2010)

A $Fe_{48}Cr_{15}Mo_{14}C_{15}B_6Y_2$ alloy with high glass forming ability (GFA) was selected to prepare amorphous metallic coatings by atmospheric plasma spraying (APS). The as-deposited coatings present a dense layered structure and low porosity. Microstructural studies show that some nanocrystals and a fraction of yttrium oxides formed during spraying, which induced the amorphous fraction of the coatings decreasing to 69% compared with amorphous alloy ribbons of the same component. High thermal stability enables the amorphous coatings to work below 910 K without crystallization. The results of electrochemical measurement show that the coatings exhibit extremely wide passive region and relatively low passive current density in 3.5% NaCl and 1 mol/L HCl solutions, which illustrate their superior ability to resist localized corrosion. Moreover, the corrosion behavior of the amorphous coatings in 1 mol/L H_2SO_4 solution is similar to their performance under conditions containing chloride ions, which manifests their flexible and extensive ability to withstand aggressive environments.

Keywords atmospheric plasma spraying, electrochemical behavior, Fe-based amorphous coating, microstructure

1. Introduction

Corrosion, wear, and fracture are considered main material failure modes in engineering environments, which lead to both enormous economy lost and great injuries. In general, most of these failures originate from the material surface; thus great attention has been paid to the surface engineering field for exploring high-performance coatings on different structural materials applied to alleviate the deteriorations. During the last few decades, as a new kind of potential application material, metallic glasses have attained increasing interest because of their unique combinations of mechanical, physical, and chemical properties. In the 1990s, amorphous alloys with high glass forming ability (GFA) were developed in a number of alloy systems (Ref 1-5), which required a critical cooling rate of 1-100 K/s for glass formation. Therefore, with the focus on these alloy systems, it is expected that one can obtain amorphous metallic coatings with high amorphous phase content. These coatings are considered to withstand aggressive environments more effectively than the coatings exploited initially with limited amorphous phase content, because of their more uniform structure.

Up to now, many attempts had been made to prepare amorphous metallic coatings using different deposition methods, for example, high-velocity oxygen fuel (HVOF) spraying (Ref 6-9), plasma spraying (Ref 10-12), kinetic spraying (Ref 13-16), electrospark deposition (Ref 17), laser cladding (Ref 18), and spark plasma sintering (Ref 19). Most of the coatings show prominent properties and potential applications in expansive industrial fields, such as oil and gas production, refining, nuclear power generation, shipping, earth excavation, drilling, and tunnel boring. Among these techniques, atmospheric plasma spraying (APS) has attracted increasing attention because of the advantages of low cost, simplicity, and flexibility. In a typical plasma spraying process, feedstock powders are fed to plasma arc flow, heated and accelerated during in-flight stage, and impacted onto substrates with high velocity and temperature, and they are subsequently spread laterally and solidified rapidly. The cooling rate of

This article is an invited paper selected from presentations at the 2010 International Thermal Spray Conference and has been expanded from the original presentation. It is simultaneously published in *Thermal Spray: Global Solutions for Future Applications, Proceedings of the 2010 International Thermal Spray Conference,* Singapore, May 3-5, 2010, Basil R. Marple, Arvind Agarwal, Margaret M. Hyland, Yuk-Chiu Lau, Chang-Jiu Li, Rogerio S. Lima, and Ghislain Montavon, Ed., ASM International, Materials Park, OH, 2011.

Z. Zhou, College of Materials Science and Engineering, Beijing University of Technology, Beijing 100124, China and School of Materials Science and Engineering, Beijing Institute of Technology, Beijing 100081, China; **D.Y. He**, College of Materials Science and Engineering, Beijing University of Technology, Beijing 100124, China; and **L. Wang, F.C. Wang,** and **Y.B. Liu**, School of Materials Science and Engineering, Beijing Institute of Technology, Beijing 100081, China. Contact e-mail: zhouzhengbjut@bjut.edu.cn.

single typical particle can achieve 10^7 to 10^8 K/s (Ref 20), which is sufficient for glass phase formation, especially for the alloy systems with high GFA. Accordingly, the fabrication of amorphous coatings possessing high amorphous phase content by means of APS technique exhibits great potential.

Fe-based amorphous metallic glasses are considered to be extremely viable candidates as surface protective coatings on account of their high crystallization temperature, superior corrosion and wear resistance, good magnetic properties, and relatively low material cost (Ref 21-23). Recently, a series of Fe-based bulk metallic glasses with high GFA were found in Fe-Cr-Mo-C-B alloy system (Ref 24), which provides a kind of selective material to obtain high amorphous fraction coatings via thermal spraying processes for satisfying engineering needs. In an earlier work, the alloy with nominal composition of $Fe_{48}Cr_{15}Mo_{14}C_{15}B_6Y_2$ was chosen to prepare amorphous metallic coatings using HVOF spraying (Ref 25), and it has been indicated that the coatings present excellent corrosion resistance. This work, however, planned to explore the possibility of fabricating $Fe_{48}Cr_{15}Mo_{14}C_{15}B_6Y_2$ amorphous metallic coatings with high amorphous fraction by APS. In addition, the corresponding microstructural characteristic and electrochemical behavior of the as-deposited coatings were also examined in detail.

2. Experimental Procedure

2.1 Materials Selection and Preparation

A master alloy ingot with nominal composition of $Fe_{48}Cr_{15}Mo_{14}C_{15}B_6Y_2$ was prepared from mixtures of pure Fe (99.9 mass%), Cr (99.9 mass%), Mo (99.9 mass%), C (99.9 mass%), and Y (99.9 mass%) as well as prealloyed Fe-B (20.6 mass%) ingot by induction melting in a copper crucible under argon atmosphere. From the master alloy, ribbon samples of 0.05 mm thickness and 2 mm width were produced by a single-roller melt-spinning technique for calculating amorphous phase content of the coating. Feedstock powders of the same composition were prepared by high-pressure argon gas atomization, then sieved according to conventional sieve analysis and divided into different size ranges. The as-atomized powders with particle sizes in the range of 40-80 μm were used for spraying onto the ASTM 1045 steel substrates. All the substrates were degreased by acetone, dried in air, and then grit blasted prior to deposition. The amorphous metallic coatings were fabricated by SG100 APS (SG100, Praxair, Concord, NH) gun, and the detailed spraying parameters for deposition process are presented in Table 1.

2.2 Microstructure Characterization

The microstructure of feedstock powders and as-deposited coatings was characterized by scanning electron microscopy (SEM) (FSM-5600LY, JEOL Ltd., Tokyo, Japan), energy dispersive spectroscopy (EDS), and transmission electron microscopy (TEM) (JEM-200CX, JEOL Ltd., Tokyo, Japan). Thin coating slices for TEM were first peeled from substrates by a mechanical method and ground to about 50 μm, then thinned by ion-beam milling until perforation occurred. X-ray diffraction (XRD) (X' Pert Pro MPD, PANalytical, Almelo, The Netherlands) analysis of the specimens was performed on an x-ray diffractometer (PANalytical) with Cu Kα radiation. A percentage of the porosity in the coatings was evaluated using image analysis on optical microscopy (OM) (PME3, Olympus, Nagano, Japan). Fifteen micrographs of stochastic cross sections of the coatings were taken to calculate the planar porosity by differentiating the contrast between lamellae and pores, and subsequently the average porosity of the whole coatings was calculated as an approximately statistic result. Oxygen content of the powders and detached coatings was analyzed by a nitrogen/oxygen determinator (TC600, LECO, St. Joseph, MI). The thermal stability of the samples was examined by differential scanning calorimeter (DSC) (404C, NETZSCH, Selb, Germany) in a continuous heating mode at a rate of 0.33 K/s under argon atmosphere. Simultaneously, the amorphous fraction of as-deposited coatings was calculated by comparing their crystallization enthalpy, which also obtained from DSC traces, with that of the ribbon sample as the similar method selected by other researchers (Ref 6). It is regarded as a relatively effective method to evaluate the amorphous fraction of coatings, because the initial crystalline phases of the as-deposited coatings would not generate phase transition and release heat during the crystallization process of the amorphous phase in DSC examination. That is, the amorphous content of the coatings is approximately proportional to their crystallization enthalpy.

Table 1 Spraying parameters employed in the APS process

Parameter	Condition
APS gun system	SG100
Arc current, A	800
Ar flow, SCFH	110
He flow, SCFH	30
Feed rate, rpm	3
Spraying distance, mm	80

2.3 Electrochemical Measurement

The electrochemical behavior of amorphous metallic coatings with the thickness about 350 μm was investigated by electrochemical measurement on a potentiostat/galvanostat (Model 273, EG&G, Princeton, NJ). Before the tests, the coating surfaces were polished using wet grinding until 1200 grit SiC paper, ultrasonically cleaned in acetone, washed in distilled water, and dried in air for an hour to promote reproducible results. Electrolytes used were 3.5 mass% NaCl, 1 mol/L HCl, and H_2SO_4 aqueous solutions, respectively, and all the electrolytes were not deaerated prior to testing. Electrochemical measurements were conducted in a three-electrode cell using a platinum counterelectrode and a saturated calomel reference electrode. The working electrode was exposed only to an area

of 1 cm^2. Potentiodynamic polarization curves were measured with a potential sweep rate of 0.167 mV/s from 0.25 V below open-circuit potentials to 1.4 V in all the solutions open to air at 298 K after immersing the specimens for an hour, when the open-circuit potentials became almost steady. For comparison, cast 316L stainless steel plates and 316L stainless steel coatings sprayed by HVOF (JP5000, Praxair, Concord, NH) were selected to perform the electrochemical measurements in the same way.

3. Results and Discussion

3.1 Coating Characteristic

A typical SEM image of feedstock powders with diameters of 40-80 μm can be seen in Fig. 1. It is clearly shown that the majority of the particles produced by gas atomization are spherical or near-spherical, although some had small satellites attached. During atomization, particles with various sizes would collide with each other in the gas turbulence. Thus some small particles with a higher solidification rate would easily adhere to the molten surfaces of large particles, form an attached particle morphology (Ref 26). In addition, most of the powders exhibit a smooth surface, indicating good fluidity, which is propitious to keep the stability and uniformity during spraying.

The XRD patterns of atomized powders, melt-spun ribbon, and as-deposited coating are shown in Fig. 2. It is notable that a single broad halo peak appearing in all the samples indicates their high amorphous phase content, which is primarily attributed to the high GFA of this selective alloy composition. The high GFA for this alloy originates according to the three empirical rules for the achievement of high GFA (Ref 27). It is regarded that the alloy chosen here satisfies the three empirical rules for the stabilization of the supercooled liquid, leading to highly dense random packed atomic configurations, higher viscosity, and lower atomic diffusivity. The enhancement of atomic-level stress suppresses the nucleation and growth reactions of crystalline phases during devitrification, such as $(Fe,Cr)_{23}C_6$ phase for the case of Fe-based BMGs with high carbon content (Ref 28). Moreover, the high cooling rate of the APS process also contributes to the formation of amorphous phase in the coatings.

The typical region from cross sections of the coatings reveals their dense layered structure, as shown in Fig. 3(a), although some pores and microcracks exist, as very dark regions can be seen from the image. Generally, the big pores located between flattened droplets are mainly caused by the loosely packed layer structure or gas porosity phenomenon, while the small pores within the flattened particles originate from shrinkage porosity (Ref 29). Despite the presence of these defects, the coatings express a low porosity below 2%, which is typical of APS thermal sprayed deposits. In addition, the microcracks obviously on the top of the coatings were presumably induced by microcutting and lamellae flaking off during surface grinding, while the microcracks in the interior of the coatings were probably caused by the release of stress that arose during rapid solidification.

With the further observation of a highly magnified image, it can be detected that a fraction of heterogeneous phases emerges in the coatings after etching with aqua regia for seconds, as indicated in Fig. 3(b). Table 2 shows the EDS analysis for sections A and B marked in Fig. 3(b). It is clear that the distribution of primary elements at section A representing the largest area of the coating is similar to that of the initial alloy system, though the content of boron and carbon is not accounted for, which is attributed to the resolving ability of EDS. However, the content of Y and O dramatically increases at section B, while other elements are nearly exhausted; thus the structure of these heterogeneous phases can be ascertained as yttrium oxides. It is regarded that oxidation occurs inevitably during APS depositing metallic powders because of the extremely high-temperature and circumambient atmosphere. Also, for the Fe-based system

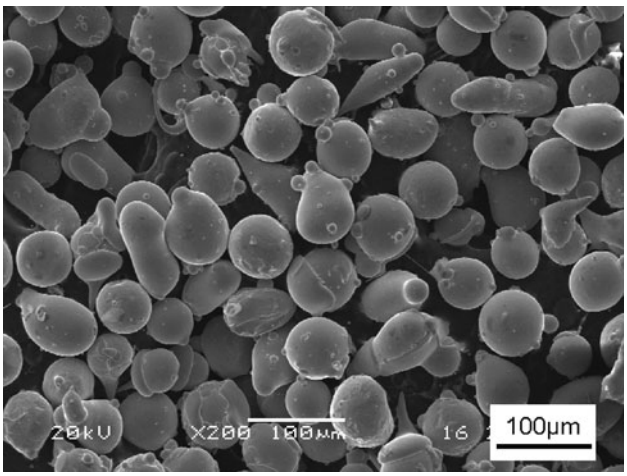

Fig. 1 Typical SEM image of $Fe_{48}Cr_{15}Mo_{14}C_{15}B_6Y_2$ alloy powders with 40-80 μm diameter

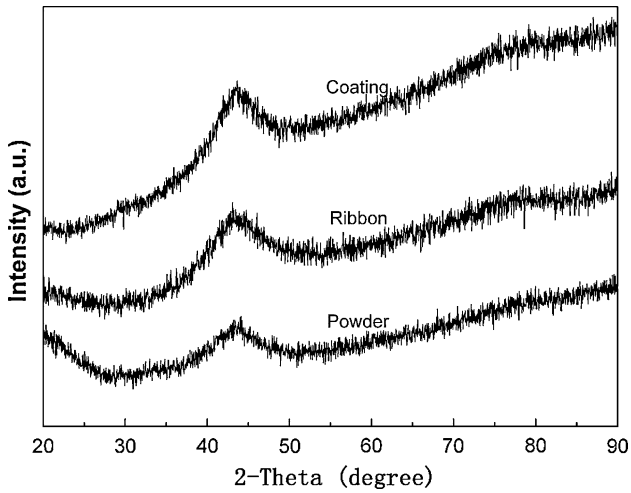

Fig. 2 XRD patterns of the melt-spun ribbon, atomized powders, and the as-deposited coatings

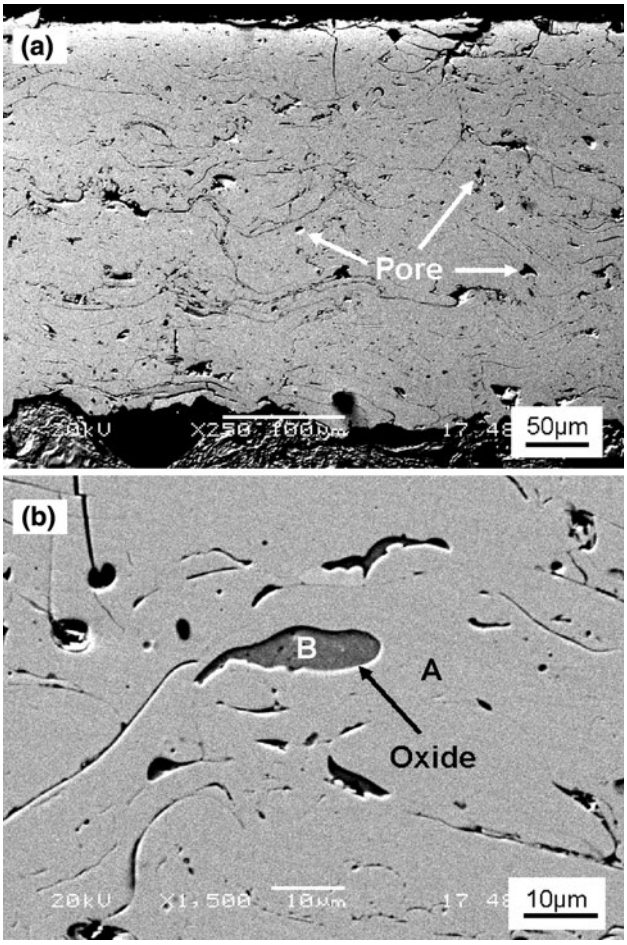

Fig. 3 SEM images of cross sections of as-deposited coating showing lamellar morphology with some pores (a) and oxides (b)

Table 2 EDS results (at.%) of section A and B in Fig. 3(b) except boron and carbon

Section	Fe	Cr	Mo	Y	O
A	63.80	19.64	14.35	2.21	…
B	…	…	…	31.92	68.08

applied now, yttrium atoms have a stronger affinity to the oxygen atoms than those of the other elements in the alloy system (Ref 30), leading to the preferential formation of yttrium oxides. Moreover, the oxygen content of the powders and detached coatings analyzed using O/N determinator, are 0.06 and 0.2 mass%, respectively; thus it could be concluded that slight oxidation occurred during the preparation of amorphous coatings by APS.

Transmission electron microscopy was undertaken to obtain more detailed information on microstructure evolution of the coatings. The diffused halo rings in the selected area diffraction (SAD) pattern show that the coatings are basically composed of amorphous phase (Fig. 4a). Nevertheless, some nanocrystalline grains with grain size in the range of 20-100 nm were distinctly

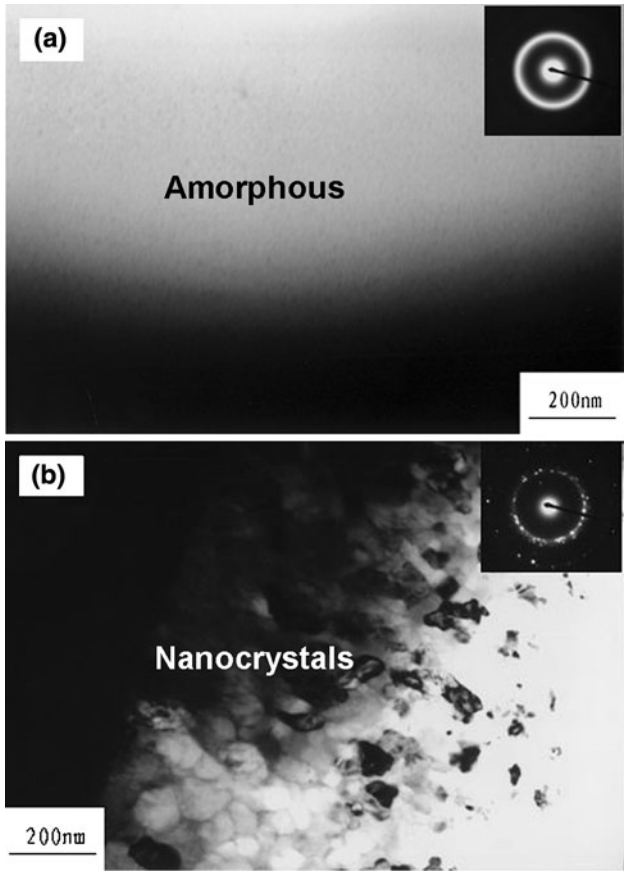

Fig. 4 Bright-field TEM images and selected area electron diffraction (SAED) patterns of as-deposited coating showing amorphous structural characteristic (a) with some nanocrystals precipitated (b)

precipitated in local microareas of the coatings, as indicated in Fig. 4(b). It is regarded that the generation of these nanocrystals is principally caused by heat accumulating inside the as-deposited coatings. To build up coatings with certain thickness, the spraying gun has to traverse the previously deposited coatings, thus lots of overlapping and connecting lamellar splats formed coatings continuously. This operation leads to localized reheating from the latent heat evolutions as successive layers of melted splats solidified. The continuous accumulation of heat increases the temperature of local regions in the coatings markedly, thus possibly enabling these regions to anneal at a high temperature over their crystallization temperature. As a result, it could be responsible for the formation of nanocrystalline grains.

To clarify the amorphous content of as-deposited coatings quantitatively, DSC traces of detached coatings, powders, and ribbon were examined as well as the crystallization enthalpy (ΔH), as shown in Fig. 5 and Table 3. The volume fraction of amorphous phase in the coatings and powders is calculated by comparing their ΔH values with that of the ribbon standard sample, which has been proved to be a fully amorphous structure by both previous work and other researchers (Ref 28). It is indicated that

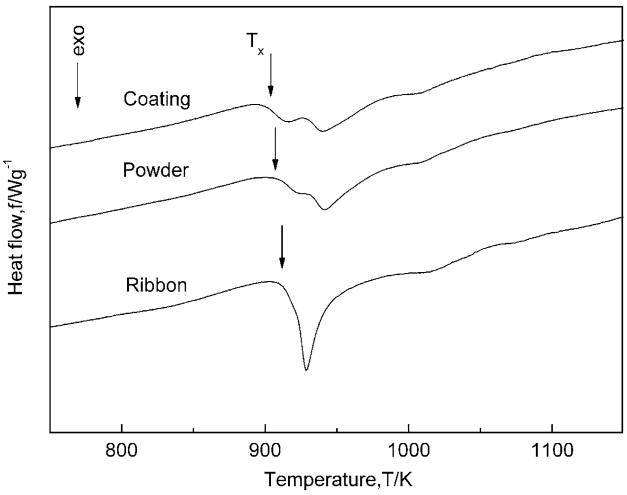

Fig. 5 DSC traces of melt-spun ribbon, atomized powders, and as-deposited coating

Table 3 Crystallization temperature (T_x), crystallization enthalpy (ΔH), and amorphous fraction (am.%) of the ribbon, powders, and coatings obtained by thermal analysis

Specimen	T_x, K	ΔH, J/g	am.%
Ribbon	920.6	−65.57	100
Powder	916.8	−49.60	75.64
Coating	913.0	−45.46	69.33

the amorphous fraction (am.%) of as-deposited coatings is nearly 70%, according to the previous conclusions that partial nanocrystals precipitated and a fraction of yttrium oxides formed during deposition. In addition, the onset crystallization temperature (T_x) of all three kind of samples are similar and exceed 910 K. In other words, the amorphous metallic coatings obtained with high thermal stability against devitrification can be used in practice reliably and widely.

3.2 Electrochemical Behavior

The potentiodynamic polarization curves of Fe-based amorphous metallic coatings compared with cast 316L stainless steel plates and HVOF sprayed 316L coatings in 3.5% NaCl, 1 mol/L HCl, and 1 mol/L H_2SO_4 aqueous solutions are indicated in Fig. 6. The corresponding corrosion parameters of amorphous coatings and 316L stainless steel materials have also been calculated and are shown in Table 4. It is apparent that the amorphous metallic coatings exhibit almost similar polarization behaviors in all the selective solutions; that is, the coatings tend to form passivation with relatively low passive current density (I_p) and retain stability with a high transpassive potential (E_{tp}) and wide passive region. Nevertheless, the

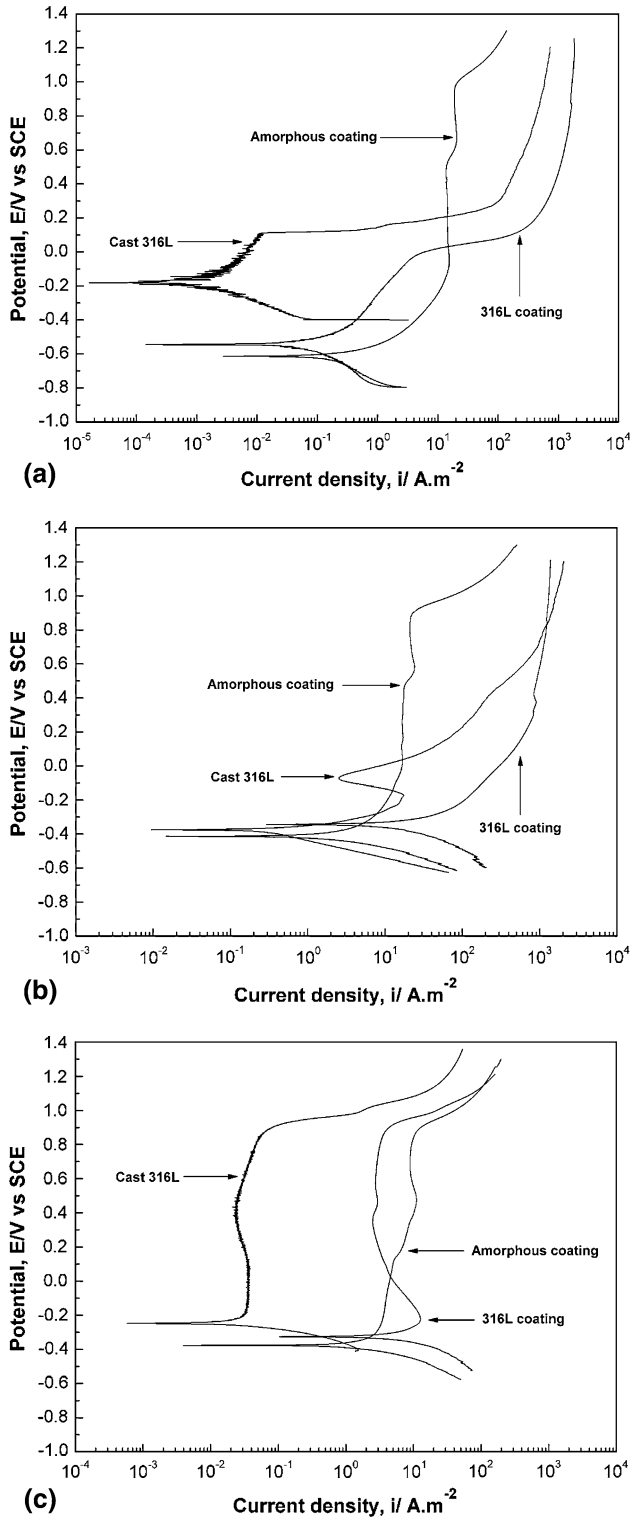

Fig. 6 Potentiodynamic polarization curves of amorphous metallic coatings, compared with cast 316L stainless steel plates and 316L coatings, in 3.5% NaCl (a), 1 mol/L HCl (b), and 1 mol/L H_2SO_4 (c) solutions open to air at 298 K

Table 4 Corrosion parameters obtained from potentiodynamic polarization curves of amorphous metallic coatings (Amor), cast 316L stainless steel plates (316L), and 316L coatings (316Lc) in 3.5% NaCl, 1 mol/L HCl, and 1 mol/L H_2SO_4 solutions

Solution/specimen	E_{corr}, mV	I_{corr}, A/m^2	I_p, A/m^2	E_{tp}, mV
NaCl				
Amor	−613.8	2.0×10^{-2}	13.4	987.6
316L	−182.2	0.03×10^{-2}	…	106.0
316Lc	−545.4	1.4×10^{-2}	…	0
HCl				
Amor	−414.1	0.11	17.2	904.3
316L	−375.3	0.05	…	−69.2
316Lc	−344.6	1.17	…	…
H_2SO_4				
Amor	−377.0	4.6×10^{-2}	5.5	879.2
316L	−247.3	0.5×10^{-2}	0.04	898.2
316Lc	−325.8	46×10^{-2}	2.96	898.2

amorphous coatings undergo a short stage of activation before passivation. This active reaction may be principally attributed to the crystals, oxides, pores, and microcracks distributing diffusely in the as-deposited coatings. These structural defects generally become the initial corrosion sites prior to the uniform amorphous matrix, leading to the rapid increase of corrosion current density at the early stage of anodic polarization, until the equilibrium of active dissolution and passivation is established.

The transpassive potential of the amorphous metallic coatings is as high as 0.9 V associating with an extremely wide passive region even in 1 mol/L HCl solution, which suggests that the coatings have a prominent ability to resist localized corrosion. In contrast, the limited or exhausted passive regions of both 316L plates and 316L coatings under conditions containing chloride ions indicate a low ability to withstand localized corrosion, such as pitting. The high resistance to localized corrosion of the amorphous metallic coatings is considered to be primarily determined by the character of forming a homogeneous phase structure without grain boundaries that are sensitive to chloride ion absorption (Ref 31). Moreover, chromium-rich passive surface films formed on Fe-Cr-based metallic glasses prevent the evolution of corrosion (Ref 22), and molybdenum improves further the corrosion resistance and passivating ability (Ref 32), since it prevents dissolution of chromium during passivation. Furthermore, the high amorphous phase content of the coatings here provides the formation of a uniform passive film and hence also contributes to their high corrosion resistance. Therefore, the performance of amorphous metallic coatings in the corrosive environments containing chloride ions to induce pitting, such as NaCl and HCl solutions, is further superior to 316L stainless steel materials.

In addition, all the samples present an excellent ability to passivate with low passive current density and almost parallel wide passive region in 1 mol/L H_2SO_4 solution. However, the passive current density of amorphous coating is comparable to that of the 316L coating, but much higher than that of the cast 316L plate in evidence. This indicates that the corrosion resistance of the amorphous coatings in 1 mol/L H_2SO_4 solution is inferior to cast 316L plates. It could be interpreted that the uncompacted structure and heterogeneous phases unfavorably affect the uniform structure of surface passive film and bear the responsibility of relatively lower corrosion resistance of the amorphous coatings. Nevertheless, it is also interesting to note that the metallic glass coatings exhibit almost similar polarization behavior in all the selective solutions as mentioned previously, whereas the 316L stainless steel does not. This means that the metallic coatings seem much more flexible, and they could be reliably employed in alternative conditions and confer the covered devices better safety against possible misuse. In any case, the excellent corrosive resistance in various conditions and the repairable feature of the Fe-based amorphous metallic coatings fabricated here endow them with potential advantage and extensively applied prospects to withstand aggressive environments.

4. Conclusions

$Fe_{48}Cr_{15}Mo_{14}C_{15}B_6Y_2$ amorphous metallic coatings with low porosity were fabricated by APS. The as-deposited coatings primarily consist of amorphous matrix because of both the high GFA of alloy system and high cooling rate of the APS process, although some nanocrystals precipitated as a result of localized reheating during successive spraying process, and a fraction of yttrium oxides also formed during deposition. These heterogeneous phases induced the amorphous fraction of the coatings decreasing to 69% compared with the ribbons of the same component.

The amorphous metallic coatings present almost similar electrochemical behavior in 3.5% NaCl, 1 mol/L HCl, and 1 mol/L H_2SO_4 aqueous solutions and exhibit excellent ability to resist localized corrosion under conditions containing chloride ions, which is further superior to 316L stainless steel materials. The uncompacted structure and existence of heterogeneous phases unfavorably affect the corrosion resistance of the amorphous coatings, leading to their performance inferior to cast 316L plates in 1 mol/L H_2SO_4 solution. However, the stable and prominent corrosion performance in various conditions of the amorphous coatings endow them with extensive potential to withstand aggressive environments.

References

1. A. Inoue, T. Zhang, and T. Masumoto, Production of Amorphous Cylinder and Sheet of La55Al25Ni20 Alloy by a Metallic Mold Casting Method, *Mater. Trans. JIM*, 1990, **31**(5), p 425-428
2. T. Zhang, A. Inoue, and T. Masumoto, Amorphous Zr-Al-TM (TM = Co, Ni, Cu) Alloys with Significant Supercooled Liquid Region of Over 100 K, *Mater. Trans. JIM*, 1991, **32**(11), p 1005-1010
3. A. Peker and W.L. Johnson, A highly Processable Metallic Glass: Zr41.2Ti13.8Cu12.5Ni10.0Be22.5, *Appl. Phys. Lett.*, 1993, **63**(17), p 2342-2344
4. A. Inoue, T. Nakamura, N. Nishiyama, and T. Masumoto, Mg-Cu-Y Bulk Amorphous Alloys with High Tensile Strength

Produced by a High-Pressure Die Casting Method, *Mater. Trans. JIM*, 1992, **33**(10), p 937-945
5. A.L. Greer, Metallic Glasses, *Science*, 1995, **267**(5206), p 1947-1953
6. A.P. Wang, X.C. Chang, W.L. Hou, and J.Q. Wang, Preparation and Corrosion Behaviour of Amorphous Ni-Based Alloy Coatings, *Mater. Sci. Eng. A*, 2007, **449-451**(25), p 277-280
7. M. Cherigui, N.E. Fenineche, and C. Coddet, Structural Study of Iron-Based Microstructured and Nanostructured Powders Sprayed by HVOF Thermal Spraying, *Surf. Coat. Technol.*, 2005, **192**(1), p 19-26
8. Y.P. Wu, P.H. Lin, G.Z. Xie, J.H. Hu, and M. Cao, Formation of Amorphous and Nanocrystalline Phases in High Velocity Oxy-Fuel Thermally Sprayed a Fe-Cr-Si-B-Mn Alloy, *Mater. Sci. Eng. A*, 2006, **430**(1-2), p 34-39
9. F.T. Parker, F.E. Spada, A.E. Berkowitz, K.S. Vecchio, E.J. Lavernia, and R. Rodriguez, Thick Amorphous Ferromagnetic Coatings via Thermal Spraying of Spark-Eroded Powder, *Mater. Lett.*, 2001, **48**(3-4), p 184-187
10. K. Kishitake, H. Era, and F. Otsubo, Characterization of Plasma Sprayed Fe-17Cr-38Mo-4C Amorphous Coatings Crystallizing at Extremely High Temperature, *J. Therm. Spray Technol.*, 1996, **5**(3), p 283-286
11. K. Kishitake, H. Era, and F. Otsubo, Thermal-Sprayed Fe-10Cr-13P-7C Amorphous Coatings Possessing Excellent Corrosion Resistance, *J. Therm. Spray Technol.*, 1996, **5**(4), p 476-482
12. F. Otsubo and K. Kishitake, Corrosion Resistance of Fe-16%Cr-30%Mo-(C, B, P) Amorphous Coatings Sprayed by HVOF and APS Processes, *Mater. Trans.*, 2005, **46**(1), p 80-83
13. H. Choi, S. Yoon, G. Kim, H. Jo, and C. Lee, Phase Evolutions of Bulk Amorphous NiTiZrSiSn Feedstock During Thermal and Kinetic Spraying Processes, *Scr. Mater.*, 2005, **53**(1), p 125-130
14. S. Yoon, H.J. Kim, and C. Lee, Deposition Behavior of Bulk Amorphous NiTiZrSiSn According to the Kinetic and Thermal Energy Levels in the Kinetic Spraying Process, *Surf. Coat. Technol.*, 2006, **200**(20-21), p 6022-6029
15. A.P. Wang, T. Zhang, and J.Q. Wang, Ni-Based Fully Amorphous Metallic Coating with High Corrosion Resistance, *Philos. Mag. Lett.*, 2006, **86**(1), p 5-11
16. B. Jodoin, P. Richer, E. Sansoucy, and E.J. Lavernia, Cold Gas Dynamic Spraying of Iron-Base Amorphous Alloy, *J. Therm. Spray Technol.*, 2006, **15**(4), p 495-500
17. S. Cadney and M. Brochu, Formation of Amorphous $Zr_{41.2}Ti_{13.8}Ni_{10}Cu_{12.5}Be_{22.5}$ Coatings via the Electrospark Deposition Process, *Intermetallics*, 2008, **16**(4), p 518-523
18. X.L. Wu and Y.S. Hong, Fe-Based Thick Amorphous-Alloy Coating by Laser Cladding, *Surf. Coat. Technol.*, 2001, **141**(2-3), p 141-144
19. A. Singh, S.R. Bakshi, A. Agarwal, and S.P. Harimkar, Microstructure and Tribological Behavior of Spark Plasma Sintered Iron-Based Amorphous Coatings, *Mater. Sci. Eng. A*, 2010, **527**(18-19), p 5000-5007
20. C. Moreau, P. Cielo, M. Lamontagne, S. Dallaire, J.C. Krapez, and M. Vardelle, Temperature Evolution of Plasma-Sprayed Niobium Particles Impacting on a Substrate, *Surf. Coat. Technol.*, 1991, **46**(2), p 173-187
21. B.L. Shen, A. Inoue, and C.T. Chang, Superhigh Strength and Good Soft-Magnetic Properties of (Fe, Co)-B-Si-Nb Bulk Glassy Alloys with High Glass-Forming Ability, *Appl. Phys. Lett.*, 2004, **85**(21), p 4911-4913
22. S.J. Pang, T. Zhang, and K. Asami, Bulk Glassy Fe-Cr-Mo-C-B Alloys with High Corrosion Resistance, *Corros. Sci.*, 2002, **44**(8), p 1847-1856
23. A. Inoue, A. Makino, and T. Mizushima, Ferromagnetic Bulk Glassy Alloys, *J. Magn. Magn. Mater.*, 2000, **215**, p 246-252
24. V. Ponnambalam, S.J. Poon, G.J. Shiflet, V.M. Keppens, R. Taylor, and G. Petculescu, Synthesis of Iron-Based Bulk Metallic Glasses as Nonferromagnetic Amorphous Steel Alloys, *Appl. Phys. Lett.*, 2003, **83**(6), p 1131-1133
25. Z. Zhou, L. Wang, F.C. Wang, H.F. Zhang, Y.B. Liu, and S.H. Xu, Formation and Corrosion Behavior of Fe-Based Amorphous Metallic Coatings by HVOF Thermal Spraying, *Surf. Coat. Technol.*, 2009, **204**(5), p 563-570
26. S. Ozbilen, Satellite Formation Mechanism in Gas Atomized Powders, *Powder Metall.*, 1999, **42**(1), p 70-78
27. A. Inoue, High Strength Bulk Amorphous Alloys with Low Critical Cooling Rates, *Mater. Trans. JIM*, 1995, **36**(7), p 866-875
28. V. Ponnambalam, S.J. Poon, and G.J. Shiflet, Fe-Based Bulk Metallic Glasses with Diameter Thickness Larger Than One Centimeter, *J. Mater. Res.*, 2004, **19**(5), p 1320-1323
29. V.V. Sobolev and J.M. Guilemany, Investigation of Coating Porosity Formation During High Velocity Oxy-Fuel (HVOF) Spraying, *Mater. Lett.*, 1994, **18**(5-6), p 304-308
30. H.K. Do, M.P. Jin, S.P. Joon, H.N. Jong, and H.K. Dong, Effect of Y Addition on Thermal Stability and the Glass Forming Ability in Fe-Nb-B-Si Bulk Glassy Alloy, *Mater. Sci. Eng. A*, 2006, **435-436**, p 425-428
31. S.J. Pang, T. Zhang, K. Asami, and A. Inoue, Synthesis of Fe-Cr-Mo-C-B-P Bulk Metallic Glasses with High Corrosion Resistance, *Acta Mater.*, 2002, **50**(3), p 489-497
32. J. Kawakita, S. Kuroda, T. Fukushima, and T. Kodama, Improvement of Corrosion Resistance of Oxyfuel-Sprayed Stainless Steel Coatings by Addition of Molybdenum, *J. Therm. Spray Technol.*, 2005, **14**(2), p 224-230